

Stress intensity factors for double-edged cracked steel beams strengthened with CFRP plates

Hai-Tao Wang^{1a}, Gang Wu^{*2}, Yu-Yang Pang^{2b} and Habeeb M. Zakari¹

¹ College of Civil and Transportation Engineering, Hohai University, Nanjing, China

² Key Laboratory of Concrete and Prestressed Concrete Structures of the Ministry of Education, Southeast University, Nanjing, China

(Received August 20, 2018, Revised April 9, 2019, Accepted November 11, 2019)

Abstract. This paper presents a theoretical and finite element (FE) study on the stress intensity factors of double-edged cracked steel beams strengthened with carbon fiber reinforced polymer (CFRP) plates. By simplifying the tension flange of the steel beam using a steel plate in tension, the solutions obtained for the stress intensity factors of the double-edged cracked steel plate strengthened with CFRP plates were used to evaluate those of the steel beam specimens. The correction factor α_1 was modified based on the transformed section method, and an additional correction factor ϕ was introduced into the expressions. Three-dimensional FE modeling was conducted to calculate the stress intensity factors. Numerous combinations of the specimen geometry, crack length, CFRP thickness and Young's modulus, adhesive thickness and shear modulus were analyzed. The numerical results were used to investigate the variations in the stress intensity factor and the additional correction factor ϕ . The proposed expressions are a function of applied stress, crack length, the ratio between the crack length and half the width of the tension flange, the stiffness ratio between the CFRP plate and tension flange, adhesive shear modulus and thickness. Finally, the proposed expressions were verified by comparing the theoretical and numerical results.

Keywords: stress intensity factor; carbon fiber reinforced polymer (CFRP); strengthening; cracked steel beam; finite element models

1. Introduction

There are numerous steel structures in infrastructures. Steel structures subjected to cyclic loading are vulnerable to fatigue damage. To prolong the service life and avoid fatigue failure of the damaged steel structures, rehabilitation is preferred to the replacement or reconstruction of the damaged structures (Wu *et al.* 2012, Hmidan *et al.* 2015). As the externally bonded carbon fiber reinforced polymer (CFRP) technique has been widely used in repairing and strengthening concrete structures in past several decades, this technique has proven to be a promising alternative to the traditional strengthening technique (Wei *et al.* 2018, Bansal *et al.* 2016, Zhang *et al.* 2018, Shen *et al.* 2019). In recent years, this technique has received much attention in strengthening steel structures (Sallam *et al.* 2010, Serror *et al.* 2017, Wang and Wu 2018a, Setvati and Mustaffa 2018, Mechab *et al.* 2016, Yu *et al.* 2019, Hosseini *et al.* 2019, Ghafoori *et al.* 2015, 2018). To evaluate the effectiveness of this technique on improving the fatigue behavior, many experimental studies have been conducted on the fatigue behavior of CFRP-strengthened steel plates (Abd-Elhady and Sallam 2017, Hosseini *et al.* 2017, Yu *et al.* 2013, Wang *et al.* 2016a, Liu *et al.* 2009a) and steel beams (Jiao *et al.*

2012, Ghafoori *et al.* 2012, Colombi and Fava 2015, Yu and Wu 2018, Ye *et al.* 2018). Effects of some factors on the strengthening effectiveness were investigated, such as the initial damage degree, CFRP configuration and system, CFRP thickness and Young's modulus, the ratio of adhesive thickness to CFRP thickness, initial crack type, single-/double-sided repair, prestress level, and so on. The results indicate that the externally bonded CFRP laminates can significantly decrease the crack growth rate and extend the fatigue life of steel members. Moreover, this technique is more effective than the traditional welding method in improving the fatigue behavior of steel structures (Wu *et al.* 2012, Jiao *et al.* 2012).

For a cracked steel member, an important parameter determining the crack growth is the stress intensity factor, which characterizes the magnitude of the singular stress field near the crack tip. Once the values of the stress intensity factor are known, the crack growth behavior can be predicted based on the crack growth laws of linear elastic fracture mechanics (Lee and Lee 2004, Albrecht *et al.* 2008, Liu *et al.* 2009b, Mall and Conley 2009, Hu *et al.* 2016, Wang *et al.* 2016a). Therefore, calculations on the stress intensity factor of CFRP-strengthened steel members are essential for the fatigue strengthening of cracked steel members. Due to the complexity in the exactly theoretical derivations of the stress intensity factor, currently, the values of the stress intensity factor for CFRP-strengthened cracked steel members are mainly calculated by numerical methods. Many finite element (FE) and boundary element (BE) models have been developed to investigate the stress

*Corresponding author, Professor,
E-mail: g.wu@seu.edu.cn

^a Associate professor

^b Ph.D. Student

intensity factors (Sun *et al.* 1996, Naboulsi and Mall 1996, Lam *et al.* 2010, Zheng 2007, Wang *et al.* 2014, Liu *et al.* 2009c, Yu *et al.* 2014a). By using numerical methods, the effects of various parameters on the stress intensity factor has been investigated (Zheng 2007, Wang *et al.* 2014, Liu *et al.* 2009c, Yu *et al.* 2014a, Colombi *et al.* 2003, El-Emam *et al.* 2017).

Nevertheless, numerical methods are sometimes time-consuming and inconvenient for predicting the fatigue crack growth because the stress intensity factors at different crack lengths usually need to be calculated (Colombi and Fava 2015, Lee and Lee 2004, Zheng 2007, Wang *et al.* 2014, Wang and Wu 2018b). If the theoretical solutions of the stress intensity factors can be derived, the crack growth behavior can be efficiently predicted. For members with simple crack configurations and loading, the stress intensity factor solutions have been presented in several handbooks (Sih 1973, China Aviation Academy 1981). However, the studies on the solutions for CFRP-strengthened cracked members are rather limited to date. The solutions of the stress intensity factor for the cracked plates strengthened with CFRP laminates have been proposed in several studies (Zheng 2007, Rose and Wang 2002, Wu *et al.* 2013, Yu *et al.* 2014b, Shen and Hou 2011, Wang *et al.* 2018). For CFRP-strengthened cracked steel beams, two types of the initial crack were commonly used in experimental studies. One type was the double-edged cracks, which were cut in the tension flange of the steel beam in order to generate initial flange cracks (Wu *et al.* 2012, Ye *et al.* 2018). The other type of the initial crack went through the tension flange and part of the web in order to generate the initial web crack (Jiao *et al.* 2012, Ghafoori *et al.* 2012, Colombi and Fava 2015, Yu and Wu 2018). For CFRP-strengthened cracked steel beams with a web crack, the equations of the stress intensity factor have also been reported in the literature (Hmidan *et al.* 2015, Ghafoori and Motavalli 2011). However, to the best knowledge of the authors, the stress intensity factor solutions for double-edged cracked steel beams strengthened with CFRP plates are still scarce.

As an extension of the previous studies conducted by authors (Wu *et al.* 2012, Wang and Wu 2018b), this paper carried out the theoretical and numerical studies on the stress intensity factors of double-edged cracked steel beams strengthened with CFRP plates. Theoretical expressions of the stress intensity factors were proposed through simply theoretical derivations. The FE simulations were used to

conduct the parametrical investigations and then calibrate the additional correction factor φ . The proposed expressions are expected to predict the fatigue crack growth of CFRP-strengthened double-edged cracked steel beams based on the crack growth laws of linear elastic fracture mechanics.

2. Geometry of the specimens

In this study, the standard hot-rolled H-shape steel beam in accordance with Chinese code (GB 50017 2003) was selected to generate the specimens. Fig. 1 shows the geometrical schematic of the specimens. The sectional height and width of the beam are h and $2b$, respectively. The thicknesses of the flange and web are t_1 and t_2 , respectively. Two through-thickness edged cracks were created in two sides of the tension flange. The length of each edged crack is a . A previous study (Wang and Wu 2018b) conducted by the authors showed that the fatigue crack growth life of the CFRP-strengthened double-edged cracked steel beam could be approximately predicted by assuming that the double-edged cracks propagated symmetrically. Therefore, an ideal double-edged crack in the tension flange of the beam was chosen in this study. The specimens were strengthened with unidirectional pultruded CFRP plates. The CFRP plates were bonded on the soffit of the tension flange. The CFRP bond length is l_f , and the bond width is the same as the width of the steel beam, i.e., $2b$. The uniform adhesive layer was assumed, and the thickness is t_a . The specimens were simply supported, and the clear span is l_n . The steel beams are loaded under four-point bending, and the distance between the two loaded points is l_d . The applied load at each load point is $P/2$.

3. Analytical study on the stress intensity factor

3.1 Background

According to the linear elastic fracture mechanics, the stress intensity factor at the crack tip of a central crack in an infinite plate can be expressed by

$$K = \sigma_0 \sqrt{\pi a} \quad (1)$$

where K is the stress intensity factor in the fracture mode I; σ_0 is the remote-field tension stress applied on the steel

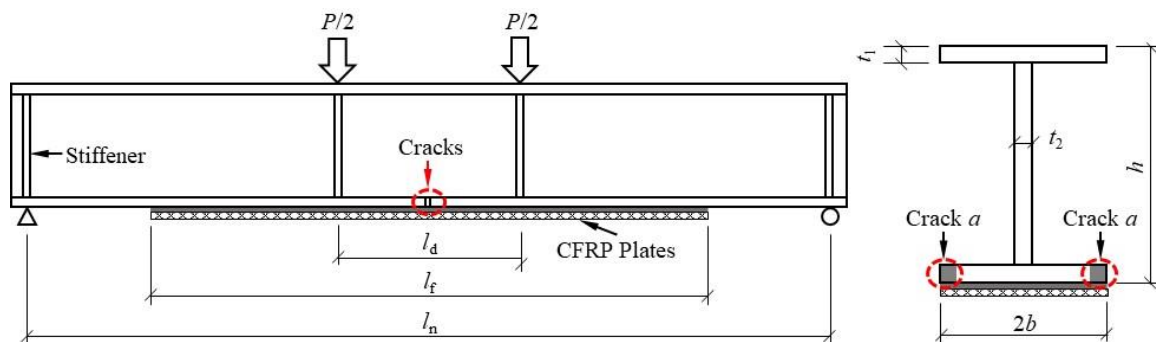


Fig. 1 The geometric schematic of the specimen

plate; and a is one-half of the central crack length.

For some finite cracked members with simple crack configurations and loadings, the stress intensity factors can be calculated according to the stress intensity factor handbooks (China Aviation Academy 1981). The unified expression for the stress intensity factor is given by

$$K = f\sigma_0\sqrt{\pi a} \quad (2)$$

where f is the correction factor to the solution of a central crack in an infinite plate under tension and a denotes the crack size. The values of the stress intensity factor for the finite cracked members can be derived by multiplying the values of the stress intensity factor for the infinite center-cracked plate by the correction factor f . Therefore, the stress intensity factor solution of the infinite center-cracked plate can serve as the fundamental part of the stress intensity factor solution of the other cracked members. Based on this concept, the stress intensity factor solution for the infinite center-cracked steel plate strengthened with CFRP plates may serve as the fundamental part of that for the CFRP-strengthened cracked steel members. Hence, the stress intensity factor solution of the infinite center-cracked steel

plate strengthened with CFRP plates is presented first. Fig. 2 shows the schematic of an infinite center-cracked steel plate strengthened with CFRP plates.

Under remote-field tension stress, the stress intensity factor at the half-crack length of a can be evaluated by the following equation (Rose and Wang 2002, Zheng 2007)

$$K = \alpha_1 \cdot \alpha_2 \cdot \sigma_0\sqrt{\pi a} \quad (3)$$

where

$$\alpha_1 = \frac{1}{1+S} \quad (4)$$

$$\alpha_2 = \sqrt{\frac{c}{a+c}} \quad (5)$$

where S is the stiffness ratio between the CFRP plate and steel plate and c is a coefficient. The coefficients S and c are expressed by

$$S = \frac{E_f t_f}{E_s t_s} \quad (6)$$

$$c = \frac{1+S}{S} \frac{1-\nu_s^2}{\pi \lambda} \quad (7)$$

where E_f and t_f are the Young's modulus and thickness of the CFRP plate bonded on each side, respectively; E_s and t_s are the Young's modulus and half-thickness of the steel plate, respectively; and ν_s is the Poisson's ratio of steel. It is noted that the effect of the adhesive layer on the stiffness ratio is not considered in Eq. (6) due to the rather low stiffness of the adhesive compared with the steel and CFRP plates. The coefficient λ can be expressed by

$$\lambda = \sqrt{\frac{G_a}{t_a} \left(\frac{1-\nu_f^2}{E_f t_f} + \frac{1-\nu_s^2}{E_s t_s} \right)} \quad (8)$$

where G_a and t_a are the shear modulus and thickness of the adhesive, respectively, and ν_f is the Poisson's ratio of the CFRP plate.

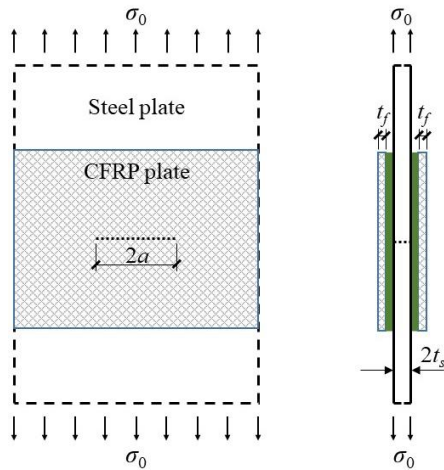
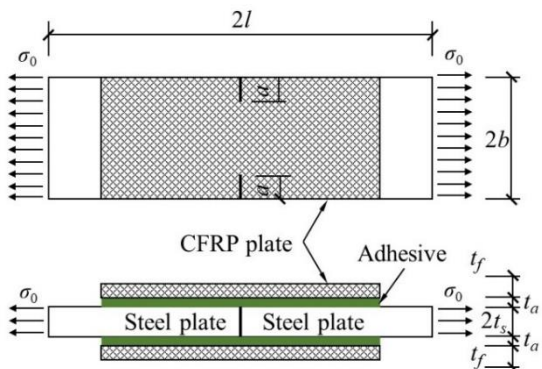
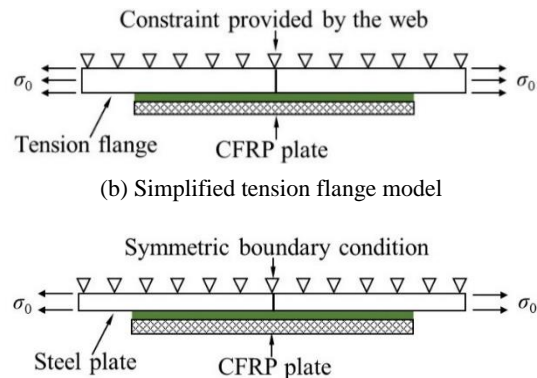


Fig. 2 The schematic of an infinite center-cracked steel plate strengthened with CFRP plates



(a) CFRP-strengthened double-edged cracked steel plate



(c) Half-model of the CFRP-strengthened double-edged cracked steel plate

Fig. 3 The schematics of the CFRP-strengthened steel plate and the simplified tension flange

By comparing Eq. (1) with Eq. (3), it can be found that two correction factors, i.e., α_1 and α_2 , are considered in the stress intensity factor solution of the CFRP-strengthened infinite cracked steel plates. The values of both factors are less than one, demonstrating that CFRP strengthening can reduce the stress intensity factor of the cracked steel plate. The strengthening mechanism of CFRP laminates, which includes a reduction in the stress and constraint effects on the crack opening (Wang *et al.* 2014), can be reflected by the two factors. The first factor α_1 represents the reduction effect of the remote-field tension stress, which mainly depends on the stiffness ratio S . A larger stiffness ratio S can result in smaller values of the stress intensity factor. The second factor α_2 indicates the constraint effect on the crack, which mainly depends on the crack length, the stiffness ratio S , the shear modulus and the adhesive thickness. It can be seen that the stress intensity factor can be reduced by increasing the stiffness ratio and the shear modulus and/or reducing the adhesive thickness.

For the double-edged cracked steel plate strengthened with CFRP plates, as shown in Fig. 3(a), the stress intensity factor solution has been developed in a previous study conducted by the authors (Wang *et al.* 2018). The proposed expression is given as follows

$$K = \beta \cdot \alpha_1 \cdot \alpha_2 \cdot f \cdot \sigma_0 \sqrt{\pi a} \quad (9)$$

where β and f are the correction factors to the solution of the infinite center-cracked steel plate strengthened with CFRP plates, which are expressed by

$$\beta = 1 + \left[0.187 + 0.13 \frac{a}{b} - 1.04 \left(\frac{a}{b} \right)^2 \right] S^{0.12} \quad (10)$$

$$f = \left[1 - 0.025 \left(\frac{a}{b} \right)^2 + 0.06 \left(\frac{a}{b} \right)^4 \right] \sqrt{\sec \frac{\pi a}{2b}} \quad (11)$$

where a is the crack length at each side of the double-edged cracked steel plate and b is half the width of the steel plate. It needs to be noted that Eq. (10) is available only for the condition of $S > 0$.

3.2 Stress intensity factor for double-edged cracked steel beam strengthened with CFRP plates

For an H-shape steel beam subjected to four-point bending loading, the tension flange at the pure-bending segment is similar to a steel plate under tension if the variations in the tension stress through the thickness of the tension flange are ignored. When CFRP plates are bonded on the soffit of the tension flange, the tension flange is strengthened with single-sided CFRP. However, the out-of-plane bending of the tension flange caused by the single-sided CFRP plates can be significantly reduced compared with the steel plate bonded with single-sided CFRP plates, because the web can produce a constraint effect. Therefore, the tension flange of the CFRP-strengthened steel beam could be simplified to the CFRP-strengthened steel plate, as shown in Fig. 3(b). This simplified tension flange model is

approximately equivalent to the half-model of the cracked steel plate strengthened with double-sided CFRP plates, as shown in Fig. 3(c). The difference between the two models is the boundary (constraint) conditions. As a consequence, the proposed solution of the stress intensity factor for the double-edged cracked steel plate strengthened with CFRP plates can be expected to evaluate the stress intensity factor for the double-edged cracked steel beam strengthened with CFRP plates through simple corrections.

In Eq. (9), the correction factor α_1 indicates the stress reduction effect of the CFRP-strengthened steel plate under tension. For the CFRP-strengthened steel beam, the Eq. (4) is not applicable and thus needs to be changed. The normal stress of the tension flange at the pure-bending segment for the CFRP-strengthened beam can be calculated based on the transformed section method. The CFRP plate is replaced by the equivalent steel plate based on the same stiffness and centroid, as shown in Fig. 4. The cross-sectional area of the equivalent steel plate is given by

$$A_{fs} = \frac{E_f}{E_s} \cdot A_f \quad (12)$$

where A_{fs} is the cross-sectional area of the equivalent steel plate; A_f is the cross-sectional area of the CFRP plate; and E_f and E_s are the Young's modulus of the CFRP plate and steel plate, respectively. If neglecting the adhesive layer, which has a rather low stiffness compared with the steel plate and CFRP plate, the distance between the centroid of the transformed section and the soffit of the tension flange is derived by

$$y_c = \frac{A_s y_s - A_{fs} y_{fs}}{A_s + A_{fs}} \quad (13)$$

where y_c is the distance between the centroid of the transformed section and the soffit of the tension flange; y_s is the distance between the centroid of the unstrengthened beam section and the soffit of the tension flange, i.e., $y_s = h/2$; and y_{fs} is the distance between the centroid of the equivalent steel plate section and the soffit of the tension flange, i.e., $y_{fs} = t_a + t_f/2$. The moment of inertia of the transformed section can be expressed by

$$I_c = I_s + A_s \cdot (y_s - y_c)^2 + I_{fs} + A_{fs} \cdot (y_c + y_{fs})^2 \quad (14)$$

where I_c is the moment of inertia of the transformed beam

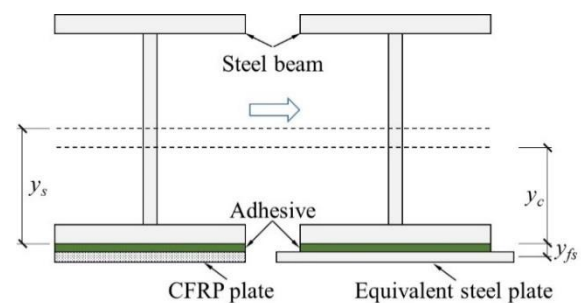


Fig. 4 The schematic of the transformed section method

section; I_s is the moment of inertia of the unstrengthened beam section; and I_{fs} is the moment of inertia of the equivalent steel plate section. The normal stress in the mid-thickness of the tension flange at the mid-span of the transformed beam section can be derived as

$$\sigma_s = \frac{M_0}{I_c} \cdot \left(y_c - \frac{t_1}{2} \right) \quad (15)$$

where σ_s is the normal stress in the mid-thickness of the tension flange at the mid-span of the transformed beam section; M_0 is the bending moment at the mid-span of the transformed beam section; and t_1 is the thickness of the tension flange.

The relationship between the normal stresses of the beam before and after strengthening can be formulated by

$$\sigma_s = \sigma_0 \cdot \frac{I_s/(y_s - t_1/2)}{I_c/(y_c - t_1/2)} \quad (16)$$

where σ_0 is the normal stress in the mid-thickness of the tension flange at the mid-span of the unstrengthened steel beam, which can be calculated by the following equation

$$\sigma_0 = \frac{M_0}{I_s} \cdot \frac{h - t_1}{2} \quad (17)$$

Therefore, the correction factor α_1 available for the double-edged cracked steel beam strengthened with CFRP plates can be written by

$$\alpha_1 = \frac{\sigma_s}{\sigma_0} = \frac{I_s/(y_s - t_1/2)}{I_c/(y_c - t_1/2)} \quad (18)$$

In the above analysis, the tension flange of the steel beam is simplified to the steel plate based on the simplifications. To offset the effects of the simplifications, an additional correction factor φ is introduced in the expression. As a result, the expression of the stress intensity factor for the double-edged cracked steel beam strengthened with CFRP plates can be given by

$$K = \varphi \cdot \beta \cdot \alpha_1 \cdot \alpha_2 \cdot f \cdot \sigma_0 \sqrt{\pi a} \quad (19)$$

where β , α_1 , α_2 , f and σ_0 are expressed by Eqs. (10), (18), (5), (11) and (17), respectively. However, the expression of the additional correction factor φ is still unknown in Eq. (19). To formulate this additional correction factor φ , the main influencing factors and the variation trends of the additional correction factor φ should be investigated first.

Table 1 The geometric details of the specimens (unit: mm)

| Specimen | 2b | h | t ₁ | t ₂ | l _n | l _f | l _d |
|------------|-----|-----|----------------|----------------|----------------|----------------|----------------|
| HM194×150 | 150 | 194 | 9 | 6 | 1400 | 1000 | 600 |
| HN350×175 | 175 | 350 | 11 | 7 | 2800 | 1500 | 500 |
| HM300×200 | 200 | 294 | 12 | 8 | 2400 | 1200 | 500 |
| HM350×250 | 250 | 340 | 14 | 9 | 2800 | 1500 | 500 |
| HW300×300* | 300 | 300 | 15 | 10 | 3200 | 1500 | 600 |
| HN450×200* | 200 | 450 | 14 | 9 | 3600 | 1500 | 600 |

*For further verification

4. Finite element modeling

The FE analysis was conducted to investigate the stress intensity factor for the double-edged cracked steel beams strengthened with CFRP plates. The FE results were used to investigate the influencing factors of the stress intensity factor and the additional correction factor φ . The expression of the additional correction factor φ was finally formulated and calibrated based on the FE results. The method for

Table 2 The analysis variables of the specimens

| Specimen | Crack length a (mm) | CFRP plate | | Adhesive | |
|------------|---|-----------------------|-------------------------|-----------------------|--------------------------|
| | | Thickness (mm) | Young' modulus (GPa) | Thickness (mm) | Shear modulus (MPa) |
| HM194×150 | 5, 10, 15, 20, 25, 30, 35, 40, 5, 50, 55, 60, 65, 70 | 1.0, 1.4, 2.0, 2.8 | 165, 210, 320, 450 | 0.5, 1.0, 1.5, 2.0 | 500, 1000, 1500, 2000 |
| HN350×175 | 5, 10, 15, 20, 25, 30, 35, 40, 45, 50, 55, 60, 65, 70, 75, 80 | 1.0, 1.4, 2.0, 2.8 | 165, 210, 320, 450 | 0.5, 1.0, 1.5, 2.0 | 500, 1000, 1500, 2000 |
| HM300×200 | 5, 10, 15, 20, 25, 30, 35, 40, 45, 50, 55, 60, 65, 70, 75, 80, 85, 90 | 1.0, 2.0 | 165, 320, 450 | 0.5, 1.0, 1.5, 2.0 | 500, 1000, 1500, 2000 |
| HM350×250 | 5, 10, 15, 20, 25, 30, 35, 40, 45, 50, 55, 60, 65, 70, 75, 80, 85, 90, 95, 100, 105, 110, 115 | 1.0, 2.0 | 165, 320, 450 | 0.5, 1.0, 1.5, 2.0 | 500, 1000, 1500, 2000 |
| HW300×300* | 5, 10, 20, 30, 40, 50, 60, 70, 80, 90, 100, 110, 120, 130 | 1.0, 2.0 | 165, 320, 450 | 1.0 | 1000 |
| HN450×200* | 5, 10, 15, 20, 25, 30, 35, 40, 45, 50, 55, 60, 65, 70, 75, 80, 85, 90 | 1.0, 2.0 | 165, 320, 450 | 1.0 | 1000 |

*For further vegrification

calibrating the correction factor based on the FE analysis has been widely used in previous studies on the stress intensity factor (Hmidan *et al.* 2015, Albrecht *et al.* 2008, Zheng 2007, Yu *et al.* 2014b, Wang *et al.* 2018, Dunn *et al.* 1997).

4.1 The geometry and material parameters of the specimens

A total of four standard hot rolled H-shape steel beams were selected for the numerical parametric study. The detailed geometrical parameters are listed in Table 1. Different crack lengths were set for each specimen to simulate the different damage degrees before strengthening. The through-thickness crack lengths changed at an interval of 5 mm for each specimen, as listed in Table 2. The effects of the CFRP thickness and Young's modulus, the adhesive thickness and the adhesive shear modulus on the stress intensity factors were analyzed. The variable values of these parameters cover a wide range, as summarized in Table 2. The existing studies showed that the CFRP bond length had no effects on the stress intensity factor when the bond length was longer than the effective bond length (Yu *et al.* 2014a). Thus, the CFRP bond length was not considered as an investigation parameter in the FE modeling because an effective bond length was usually ensured in the practical applications. The different combinations of CFRP thickness and Young's modulus can provide the different CFRP stiffnesses. The Young's modulus and the Poisson's ratio of the steel are 206 GPa and 0.3, respectively, which remained unchanged in the parametric investigations for all of the specimens. The material properties of the CFRP plate and the adhesive are listed as follows: the thickness and Young's modulus of the CFRP plate are 2.0 mm and 450 GPa, respectively; the Poisson's ratio of the CFRP plate is 0.28; the thickness and shear modulus of the adhesive are 1.0 mm and 1000 MPa, respectively; and the Poisson's ratio of the adhesive is 0.35. When one parameter was changed, the values of other parameters remained unchanged during the parametric investigations.

4.2 Finite element models

Three-dimensional (3D) linear-elastic FE models were developed using ANSYS software to obtain the stress

intensity factors of the specimens. Only one-quarter of the full-scale specimens were modeled due to the material and geometric symmetry conditions. Therefore, the symmetrical boundary conditions were applied to the nodes belonging to the symmetrical planes. The typical FE meshes are shown in Fig. 5. In the FE models, the CFRP plate and steel beam were meshed using the eight-node 3D solid element SOLID45. Mesh refinement was conducted in the vicinity of the crack tip. Twelve elements were used around the circumferential direction of the FE model, as shown in Fig. 5. The element length in the vicinity of the crack tip was set to 1/20 of the crack length based on the mesh convergence analysis. To obtain variations in the stress intensity factor through the thickness of the tension flange, the tension flange was meshed by six layers of elements. As a result, seven values of the stress intensity factor at each crack length can be obtained through the flange thickness. Assuming no relative slip at the CFRP/adhesive interface and the adhesive/steel interface, the adhesive layer was modeled using linear spring element COMBIN14. The length of the spring is equal to the thickness of the adhesive layer. By setting the parameter "KEYOPT(2) = 1, 2, and 3", the spring element can simulate the 1D longitudinal behavior in the x, y, and z directions, respectively. To simulate the axial and shear deformation of the adhesive layer, three spring elements were installed between each node pair corresponding to the CFRP/adhesive interface and the adhesive/steel interface. The shear and axial spring constants can be calculated according to the following equations (Sun *et al.* 1996)

$$K_i = \frac{G_a A_a}{t_a} \quad (20)$$

$$K_y = \frac{2(1 - \nu_a)G_a A_a}{(1 - 2\nu_a)t_a} \quad (21)$$

where K_i ($i = x, z$) and K_y are the shear and axial spring constants, respectively, and A_a is the adhesive area represented by the responding spring. The nodes of the FE models were constrained at the supported-end to represent a simply supported boundary condition. A loading of 50 kN ($P/4$) was applied to the loaded point in the model, and the linear elastic analyses were carried out.

The virtual crack closure method (Krueger 2004) was

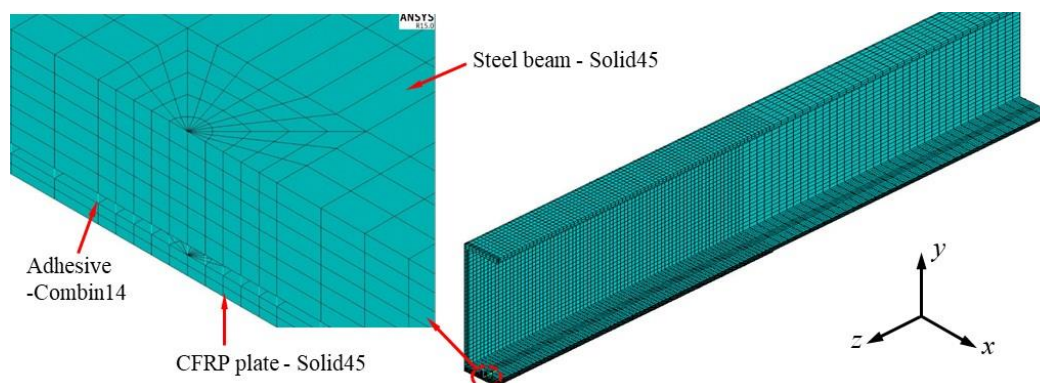


Fig. 5 Typical finite element model

used to calculate the energy release rate of the crack tip. Using this method, the quarter-point singular elements were not necessary in the models, and the results were insensitive to the FE mesh sizes (Krueger 2004, Wang *et al.* 2014). The energy release rate can be easily obtained by picking out the elemental nodal forces at the crack tip and the nodal displacements behind the crack tip. All forces and displacements were obtained from the linear-elastic FE analysis with respect to the global coordinate system. The energy release rate can be converted into the stress intensity factor as follows

$$K = \sqrt{G_I \cdot E_s} \quad (22)$$

where G_I is the energy release rate in the fracture mode I. In the subsequent analysis, the root mean square value of the stress intensity factors through the thickness of the tension flange is used as the representative value.

5. FE results and discussions

In this section, the effects of the stiffness ratio, adhesive thickness and shear modulus on the stress intensity factors were investigated based on the FE results. Because similar trends were observed for all four specimens in terms of the stress intensity factors versus the three parameters, only the results for specimen HN350×175 are presented here for analysis.

5.1 Effect of the stiffness ratio

Different combinations of CFRP thickness and Young's modulus can result in different values of the CFRP stiffness. Therefore, the stiffness ratio S between the CFRP plate and tension flange is an important parameter. Fig. 6 plots the effect of the stiffness ratio S on the stress intensity factor. In the figure, the horizontal axis is the ratio between the crack length a and half the width of the tension flange b , i.e., a/b . It is obvious that the stress intensity factors increase gradually with the increase in the value of the a/b for each of the curves. At the same a/b , the stress intensity factors are significantly reduced with the increase in the stiffness ratio S . When the a/b is 0.23 (the crack length a is 20 mm), the value of the stress intensity factor is reduced from 1068.7 MPa·mm^{1/2} to 834.6 MPa·mm^{1/2}, i.e., a reduction of 22.0%, as the stiffness ratio S increases from 0.1 to 0.4. When the a/b is 0.57 (the crack length a is 50 mm), the CFRP plates with the stiffness ratio S of 0.4 can reduce the stress intensity factors by 26.5% compared with the plates with the stiffness ratio S of 0.1. It can be concluded that an increase in the stiffness ratio S can obviously reduce the stress intensity factors.

5.2 Effect of the adhesive thickness

Fig. 7 illustrates the effect of the adhesive thickness on the stress intensity factor; the modeled adhesive thickness is 0.5 mm, 1.0 mm, 1.5 mm, and 2.0 mm. It can be seen that the stress intensity factor increases with the increase in the adhesive thickness. When the adhesive thickness increases

from 0.5 mm to 2.0 mm, the stress intensity factors are increased from 795.1 MPa·mm^{1/2} to 875.2 MPa·mm^{1/2} for the a/b of 0.23 (the crack length of 20 mm), i.e., increased by 10.1%. The stress intensity factors are increased by 11.9% for the a/b of 0.57 (the crack length of 50 mm). Therefore, a thinner adhesive results in a smaller stress intensity factor. However, one factor that should be taken into account is that a thinner adhesive would result in a lower bond strength and thus cause a risk of CFRP debonding failure based on the existing study (Wang *et al.* 2016b).

5.3 Effect of the adhesive shear modulus

To assess the influence of the adhesive shear modulus on the stress intensity factor, four specimens with different shear modulus values were designed. The adhesive shear modulus values used in the models are 500 MPa, 1000 MPa, 1500 MPa, and 2000 MPa. Fig. 8 shows the relationships between the stress intensity factors and the crack length at different shear modulus values. The results show that the stress intensity factors can be reduced by a higher adhesive shear modulus. When the a/b is 0.23 (the

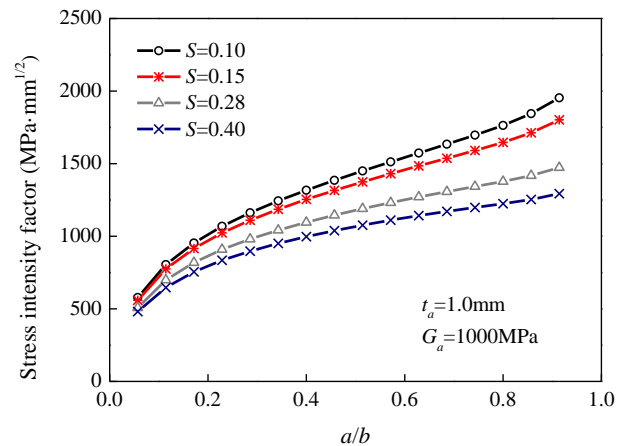


Fig. 6 Effect of the stiffness ratio on the stress intensity factor

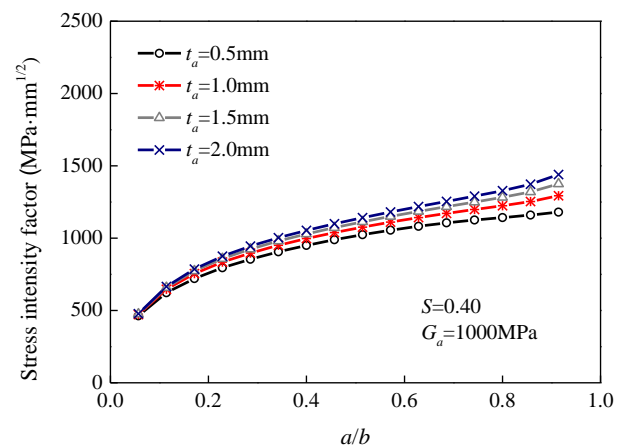


Fig. 7 Effect of the adhesive thickness on the stress intensity factor

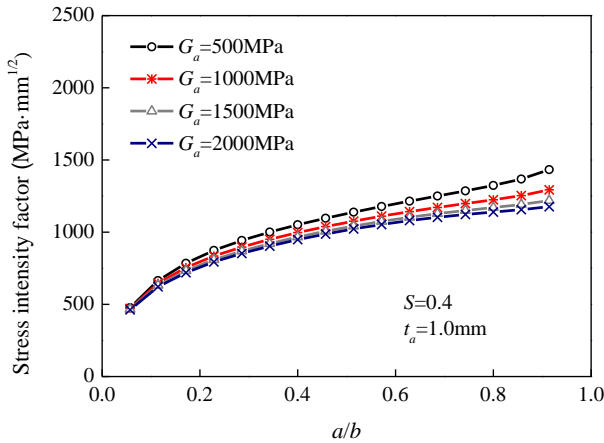


Fig. 8 Effect of the adhesive shear modulus on the stress intensity factor

crack length is 20 mm), the stress intensity factors decrease from 873.6 MPa·mm^{1/2} to 793.6 MPa·mm^{1/2}, i.e., decreased by 9.2% when the shear modulus increases from 500 MPa to 2000 MPa. When the *a/b* is 0.57 (the crack length *a* is 50 mm), the increase in the shear modulus from 500 MPa to 2000 MPa can reduce the stress intensity factors by 10.6%. Moreover, it should be noted that a high adhesive shear modulus could also cause a risk of CFRP debonding failure.

6. Development of additional correction factors φ

Based on the FE results, the additional correction factor φ can be obtained according to the following equation

$$\varphi = \frac{K_{FE}}{\beta \cdot \alpha_1 \cdot \alpha_2 \cdot f \cdot \sigma_0 \sqrt{\pi a}} \quad (23)$$

where K_{EF} denotes the values of the stress intensity factors from FE results.

Based on the aforementioned FE results and Eq. (23), the variations in the additional correction factor φ can be obtained. Fig. 9 presents the effect of the stiffness ratio *S* on the additional correction factor φ for specimen HN350×175. When the values of the *a/b* are the same, the values of the additional correction factor φ gradually increase with the increasing stiffness ratio *S*. Fig. 10 plots the effect of the adhesive thickness on the additional correction factor φ for specimen HN350×175. It can be seen that the values of the additional correction factor φ show a decreasing trend with the increasing adhesive thickness when the values of the *a/b* are same. Fig. 11 illustrates the effect of the adhesive shear modulus on the additional correction factor φ for specimen HN350×175. It can be observed that the values of the additional correction factor φ gradually increase with the increase in the adhesive shear modulus at the same *a/b* values. Moreover, the variations in the additional correction factor φ with the *a/b* can also be found in Figs. 9-11. It can be found that the values of the additional correction factor φ gradually increase and then decrease with the increase in values of the *a/b*. This transition takes place when the *a/b* is approximately 0.7. The variation trends of the additional

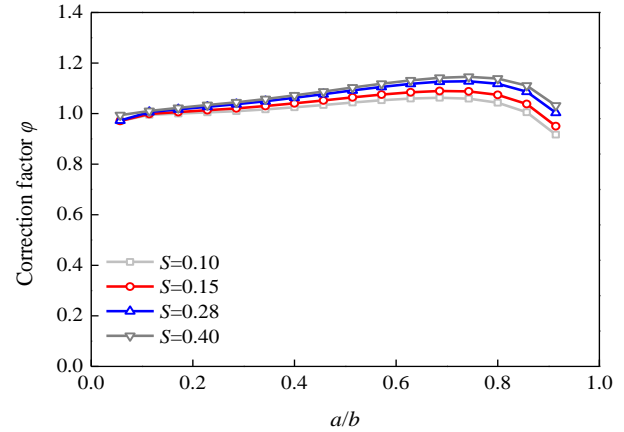


Fig. 9 Effect of the stiffness ratio on the additional correction factor φ

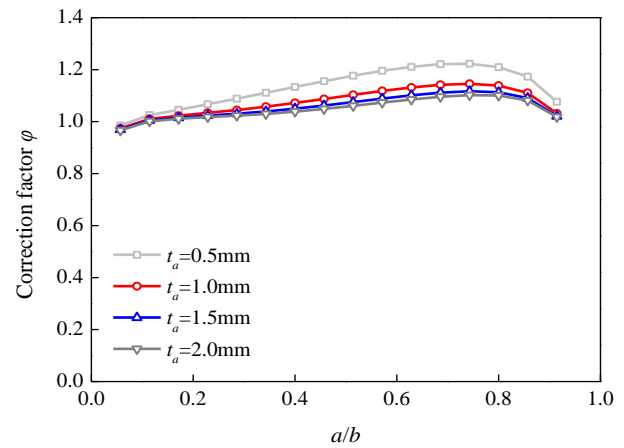


Fig. 10 Effect of the adhesive thickness on the correction factor φ

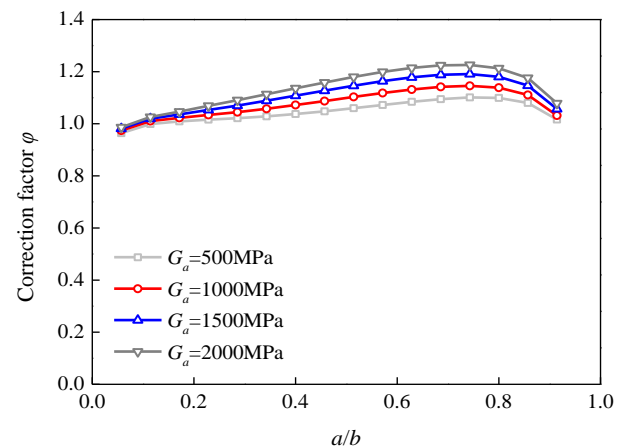


Fig. 11 Effect of the adhesive shear modulus on the correction factor φ

correction factor φ with the *a/b*, the stiffness ratio, the adhesive thickness and shear modulus for other specimens are similar to those showed in Figs. 9-11.

The analysis shows that all four parameters affect the values of the additional correction factor φ . Thus, it seems

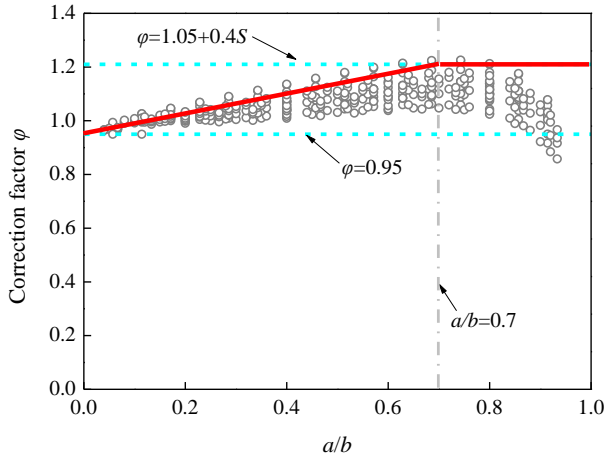


Fig. 12 Analysis of the additional correction factor ϕ

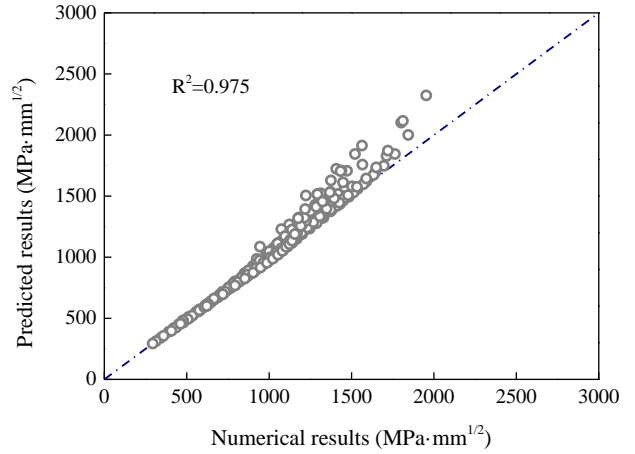
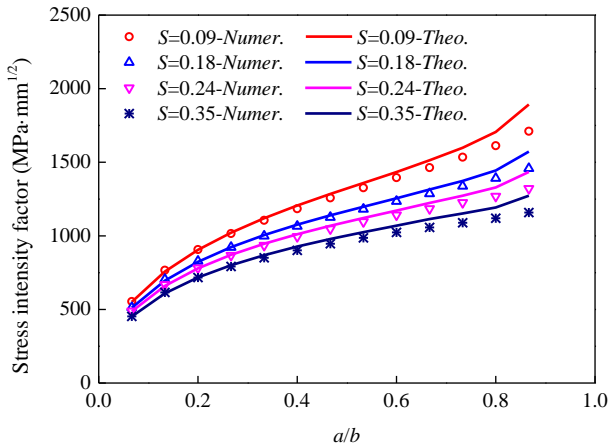


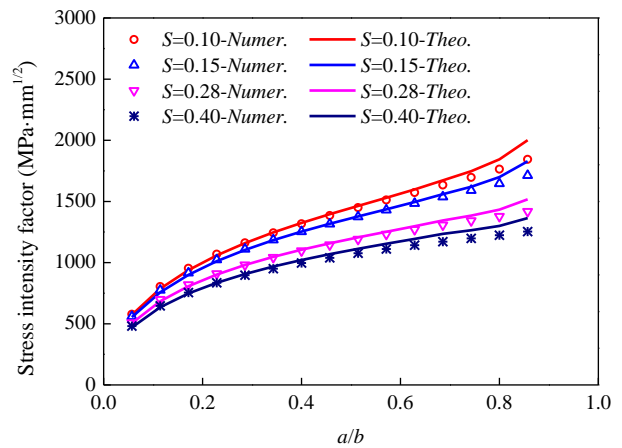
Fig. 13 Comparison of the theoretical and numerical results

to be difficult to derive an expression including the effects of the four parameters. To derive a simple expression of the additional correction factor ϕ that is conveniently used, simplified analyses are conducted. From the above FE analysis on the stress intensity factors, the stiffness ratio S and the a/b have more significant effects on the stress intensity factors compared with the adhesive properties.

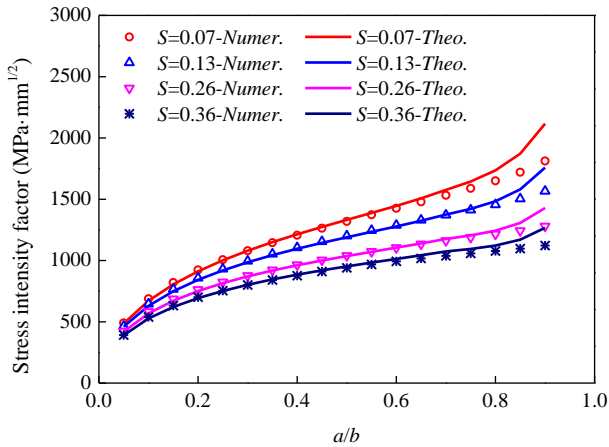
Therefore, the effects of the a/b and the stiffness ratio S are considered in the expressions. By analyzing the data, the lower bound of the values of the additional correction factor ϕ is approximately 0.95, and the upper bound can be approximately expressed by $1.05+0.4S$, as shown in Fig. 12. For the design, the values of the additional correction factor ϕ can be approximately predicted according to the solid line



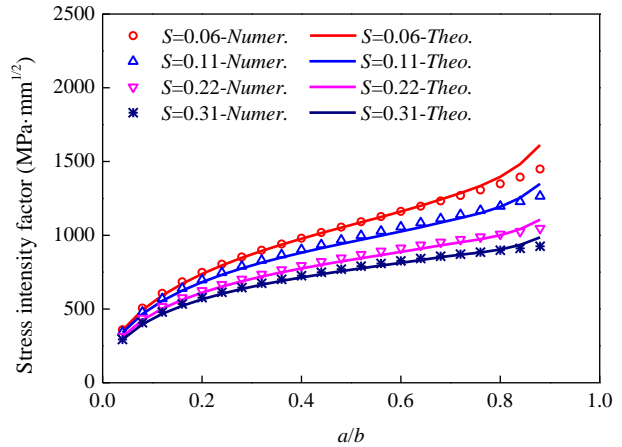
(a) Beam HM194×150



(b) Beam HN350×175



(c) Beam HM300×200



(d) Beam HM350×250

Fig. 14 Comparison of the theoretical and numerical results

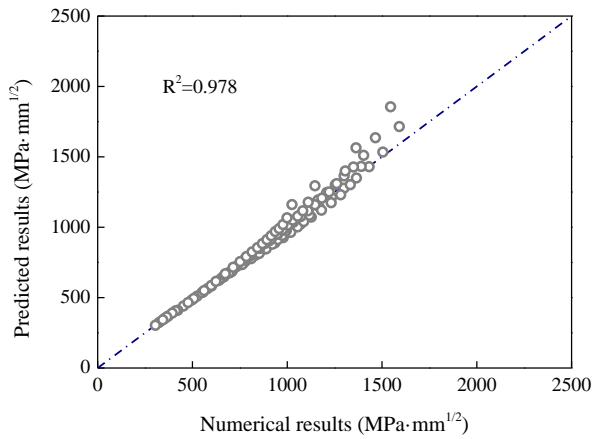


Fig. 15 Comparison of the theoretical and numerical results for two extra specimens

in Fig. 12. When the a/b is not greater than 0.7, the values of the additional correction factor ϕ are calculated by the interpolation method. When the a/b is greater than 0.7, the values of the additional correction factors ϕ are simplified to be unchanged at the upper bound. As a result, the predicted values are larger than the numerical results for most cases, which demonstrates that the predicted results are conservative. It is noted that because the fatigue issue is complicated and the accurate prediction of the fatigue life is relative difficult, a conservative expression of the additional correction factor ϕ is used in the study to calculate the stress intensity factors. Finally, a practical expression of the additional correction factor ϕ is formulated by a piecewise function as follows

$$\phi = \begin{cases} 0.95 + \left(\frac{0.1 + 0.4S}{0.7}\right) \cdot \frac{a}{b} & \frac{a}{b} \leq 0.7 \\ 1.05 + 0.4S & \frac{a}{b} > 0.7 \end{cases} \quad (24)$$

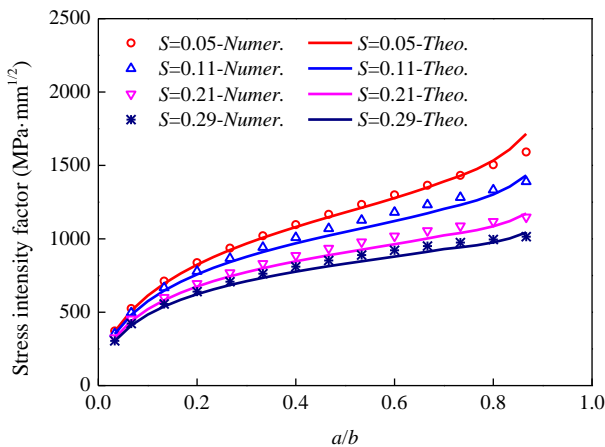
where a is the crack length at each side of the tension flange; b is the half-width of the tension flange; and S is the stiffness ratio between the CFRP plate and tension flange,

i.e., $S = E_f t_f / E_s t_1$, which is also available for Eq. (7) when the stress intensity factors of the double-edged cracked steel beam strengthened with CFRP plates are calculated.

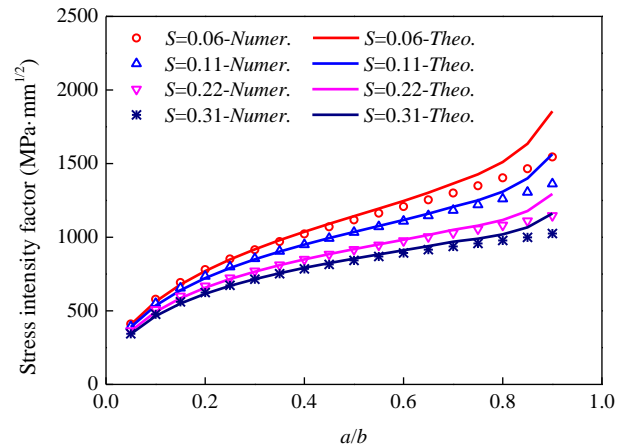
Based on the above analytical and numerical study, the theoretical expressions for the stress intensity factors are finally proposed. The stress intensity factors of the double-edged cracked steel beams strengthened with CFRP plates can be calculated using Eqs. (5), (10), (11), (17), (18), (19), and (24). It can be seen that the proposed expressions are a function of the applied stress, the crack length, the ratio between the crack length and half the width of the tension flange, the stiffness ratio between the CFRP plate and the tension flange, the adhesive shear modulus and thickness.

7. Verification of the proposed equations

According to the proposed equations, the stress intensity factors of the specimens can be calculated. Figs. 13-14 plot the comparisons of the theoretical and numerical results for the four specimens. It can be seen that the theoretical results agree well with the numerical results for all specimens at different values of the stiffness ratio S . The mean of the ratios between the theoretical and numerical results for all specimens is 1.02, and the coefficient of variation (COV) is 0.05. It can be observed that the theoretical results are larger than the numerical results when the fatigue crack is long. However, the steel beams have been substantially damaged by cracks and are approaching failure in this stage. Thus, the overestimations of the stress intensity factors have little effect on the crack growth life of the member and can make the predicted crack growth lives conservative and make the design safe. To further verify the proposed formulas, two extra specimens, i.e., HW300×300 and HN450×200, were modeled. The detailed parameters of the two specimens are listed in Tables 1 and 2, respectively. Figs. 15-16 show the comparisons of the theoretical and numerical results for both specimens. It can be seen that the theoretical results also agree well with the numerical results. The mean of the ratios between the theoretical and numerical results for the two specimens is 1.01, and the COV is 0.04. The above comparisons demonstrate that the proposed equations can



(a) Beam HW300×300



(b) Beam HN450×200

Fig. 16 Comparison of the theoretical and numerical results for two extra specimens

calculate the stress intensity factors of the double-edged cracked steel beams strengthened with CFRP plates with reasonable accuracy.

8. Conclusions

The theoretical and numerical study was conducted to investigate the stress intensity factors for the double-edged cracked steel beams strengthened with CFRP plates. The expressions of the stress intensity factor were proposed by modifying the expressions for CFRP-strengthened double-edged cracked steel plates. The expression of the correction factor α_1 was derived based on the transformed section method. The main influencing factors of the additional correction factor φ were investigated by the FE analysis. Results show that the four parameters, i.e., the a/b , stiffness ratio S , adhesive shear modulus and thickness, have effects on the values of the additional correction factor φ . The simplified expression of the additional correction factor φ was formulated based on the parametric investigations. The stress intensity factors for the double-edged cracked steel beams strengthened with CFRP plates can be calculated based on the proposed Eqs. (5), (10), (11), (17), (18), (19) and (24). The comparisons of the theoretical and numerical results indicate the proposed expressions can predict the stress intensity factors with reasonable accuracy.

Acknowledgments

The authors would like to acknowledge the financial support from the National Natural Science Foundation of China (51708174), Jiangsu Natural Science Foundation (BK20170889), Project Funded by China Postdoctoral Science Foundation (2019M651675), and the Fundamental Research Funds for the Central Universities (2017B00714).

References

- Abd-Elhady, A.A. and Sallam, H.E.M. (2017), "Discussion of 'Fatigue Behavior of Cracked Steel Plates Strengthened with Different CFRP Systems and Configurations' by Hai-Tao Wang, Gang Wu, and Jian-Biao Jiang", *J. Compos. Constr.*, **21**(3), 07016002.
[https://doi.org/10.1061/\(ASCE\)CC.1943-5614.0000767](https://doi.org/10.1061/(ASCE)CC.1943-5614.0000767)
- Albrecht, P., Lenwari, A. and Feng, D.Q. (2008), "Stress intensity factors for structural steel I-beams", *J. Struct. Eng.*, **134**(3), 421-429.
[https://doi.org/10.1061/\(ASCE\)0733-9445\(2008\)134:3\(421\)](https://doi.org/10.1061/(ASCE)0733-9445(2008)134:3(421))
- Bansal, P.P., Sharma, R. and Mehta, A. (2016), "Retrofitting of RC girders using pre-stressed CFRP sheets", *Steel Compos. Struct.*, **Int. J.**, **20**(4), 833-849.
<https://doi.org/10.12989/scs.2016.20.4.833>
- China Aviation Academy (1981), *Stress Intensity Factor Handbook*, Science Press, Beijing, China.
- Colombi, P. and Fava, G. (2015), "Experimental study on the fatigue behaviour of cracked steel beams repaired with CFRP plates", *Eng. Fract. Mech.*, **145**, 128-142.
<https://doi.org/10.1016/j.engfracmech.2015.04.009>
- Colombi, C., Bassetti, A. and Nussbaumer, A. (2003), "Analysis of cracked steel members reinforced by pre-stress composite patch", *Fatigue Fract. Eng. M.*, **26**(1), 59-66.
<https://doi.org/10.1046/j.1460-2695.2003.00598.x>
- Dunn, M.L., Suwito, W. and Hunter, B. (1997), "Stress intensity factor for cracked I-beams", *Eng. Fract. Mech.*, **57**(6), 609-616.
[https://doi.org/10.1016/S0013-7944\(97\)00059-3](https://doi.org/10.1016/S0013-7944(97)00059-3)
- El-Emam, H.M., Salim, H.A. and Sallam, H.E. (2017), "Composite patch configuration and prestress effect on SIFs for inclined cracks in steel plates", *J. Struct. Eng.*, **143**(5), 04016229.
[https://doi.org/10.1061/\(ASCE\)ST.1943-541X.0001727](https://doi.org/10.1061/(ASCE)ST.1943-541X.0001727)
- GB 50017 (2003), Code for design of steel structures; China Planning Press, Beijing, China.
- Ghafoori, E. and Motavalli, M. (2011), "Analytical calculation of stress intensity factor of cracked steel I-beams with experimental analysis and 3D digital image correlation measurements", *Eng. Fract. Mech.*, **78**(18), 3226-3242.
<https://doi.org/10.1016/j.engfracmech.2011.09.012>
- Ghafoori, E., Motavalli, M., Botsis, J., Herwig, A. and Galli, M. (2012), "Fatigue strengthening of damaged metallic beams using prestressed unbonded and bonded CFRP plates", *Int. J. Fatigue*, **44**, 303-315. <https://doi.org/10.1016/j.ijfatigue.2012.03.006>
- Ghafoori, E., Motavalli, M., Nussbaumer, A., Herwig, A., Prinz, G.S. and Fontana, M. (2015), "Design criterion for fatigue strengthening of riveted beams in a 120-year-old railway metallic bridge using pre-stressed CFRP plates", *Compos. B: Eng.*, **68**, 1-13.
<https://doi.org/10.1016/j.compositesb.2014.08.026>
- Ghafoori, E., Hosseini, A., Al-Mahaidi, R., Zhao, X.L. and Motavalli, M. (2018), "Prestressed CFRP-strengthening and long-term wireless monitoring of an old roadway metallic bridge", *Eng. Struct.*, **176**, 585-605.
<https://doi.org/10.1016/j.engstruct.2018.09.042>
- Hmidan, A., Kim, Y.J. and Yazdani, S. (2015), "Stress intensity factors for cracked steel girders strengthened with CFRP sheets", *J. Compos. Constr.*, **19**(5), 04014085.
[https://doi.org/10.1061/\(ASCE\)CC.1943-5614.0000552](https://doi.org/10.1061/(ASCE)CC.1943-5614.0000552)
- Hosseini, A., Ghafoori, E., Al-Mahaidi, R., Zhao, X.L. and Motavalli, M. (2019), "Strengthening of a 19th-century roadway metallic bridge using nonprestressed bonded and prestressed unbonded CFRP plates", *Constr. Build. Mater.*, **209**, 240-259.
<https://doi.org/10.1016/j.conbuildmat.2019.03.095>
- Hosseini, A., Ghafoori, E., Motavalli, M., Nussbaumer, A. and Zhao, X.L. (2017), "Mode I fatigue crack arrest in tensile steel members using prestressed CFRP plates", *Compos. Struct.*, **178**, 119-134. <https://doi.org/10.1016/j.compstruct.2017.06.056>
- Hu, L.L., Zhao, X.L. and Feng, P. (2016), "Fatigue behavior of cracked high-strength steel plates strengthened by CFRP sheets", *J. Compos. Constr.*, **20**(6), 04016043.
[https://doi.org/10.1061/\(ASCE\)CC.1943-5614.0000698](https://doi.org/10.1061/(ASCE)CC.1943-5614.0000698)
- Jiao, H., Mashiri, F. and Zhao, X.L. (2012), "A comparative study on fatigue behaviour of steel beams retrofitted with welding, pultruded CFRP plates and wet layup CFRP sheets", *Thin-Wall. Struct.*, **59**, 144-152. <https://doi.org/10.1016/j.tws.2012.06.002>
- Krueger, R. (2004), "Virtual crack closure technique: History, approach, and applications", *Appl. Mech. Rev.*, **57**(2), 109-143.
<https://doi.org/10.1115/1.1595677>
- Lam, A.C.C., Yam, M.C.H., Cheng, J.J.R. and Kennedy, G.D. (2010), "Study of stress intensity factor of a cracked steel plate with a single-side CFRP composite patching", *J. Compos. Constr.*, **14**(6), 791-615.
[https://doi.org/10.1061/\(ASCE\)CC.1943-5614.0000136](https://doi.org/10.1061/(ASCE)CC.1943-5614.0000136)
- Lee, W.Y. and Lee, J.J. (2004), "Successive 3D FE analysis technique for characterization of fatigue crack growth behavior in composite-repaired aluminum plate", *Compos. Struct.*, **66**(1-4), 513-520. <https://doi.org/10.1016/j.compstruct.2004.04.074>
- Liu, H.B., Al-Mahaidi, R. and Zhao, X.L. (2009a), "Experimental study of fatigue crack growth behaviour in adhesively reinforced

- steel structures”, *Compos. Struct.*, **90**(1), 12-20.
<https://doi.org/10.1016/j.compstruct.2009.02.016>
- Liu, H.B., Xiao, Z.G., Zhao, X.L. and Al-Mahaidi, R. (2009b), “Prediction of fatigue life for CFRP-strengthened steel plates”, *Thin-Wall. Struct.*, **47**(10), 1069-1077.
<https://doi.org/10.1016/j.tws.2008.10.011>
- Liu, H.B., Zhao, X.L. and Al-Mahaidi, R. (2009c), “Boundary element analysis of CFRP reinforced steel plates”, *Compos. Struct.*, **91**(1), 74-83.
<https://doi.org/10.1016/j.compstruct.2009.04.032>
- Mall, S. and Conley, D.S. (2009), “Modeling and validation of composite patch repair to cracked thick and thin metallic panels”, *Compos. Part A*, **40**(9), 1331-1339.
<https://doi.org/10.1016/j.compositesa.2008.08.007>
- Mechab, B., Chama, M., Kaddouri, K. and Slimani, D. (2016), “Probabilistic elastic-plastic analysis of repaired cracks with bonded composite patch”, *Steel Compos. Struct., Int. J.*, **20**(6), 1173-1182. <https://doi.org/10.12989/scs.2016.20.6.1173>
- Naboulsi, S. and Mall, S. (1996), “Modeling of a cracked metallic structure with bonded composite patch using the three layers technique”, *Compos. Struct.*, **35**(3), 295-308.
[https://doi.org/10.1016/0263-8223\(96\)00043-8](https://doi.org/10.1016/0263-8223(96)00043-8)
- Rose, L.R.F. and Wang, C.H. (2002), “Analytical Methods for Designing Composite Repairs”, In: Baker, A.A., Rose, L.R.F. and Jones, R. (Eds.), *Advances in Bonded Composite Repairs of Metallic Airframe Structure*, Elsevier Science Ltd., Amsterdam, Netherlands.
- Sallam, H.E.M., Badawy, A.A.M., Saba, A.M. and Mikhail, F.A. (2010), “Flexural behavior of strengthened steel-concrete composite beams by various plating methods”, *J. Const. Steel Res.*, **66**(8-9), 1081-1087.
<https://doi.org/10.1016/j.jcsr.2010.03.005>
- Serror, M.H., Soliman, E.G. and Hassan, A.F. (2017), “Numerical study on the rotation capacity of CFRP strengthened cold formed steel beams”, *Steel Compos. Struct., Int. J.*, **23**(4), 385-397.
<https://doi.org/10.12989/scs.2017.23.4.385>
- Setvati, M.R. and Mustaffa, R. (2018), “Rehabilitation of notched circular hollow sectional steel beam using CFRP patch”, *Steel Compos. Struct., Int. J.*, **26**(2), 151-161.
<https://doi.org/10.12989/scs.2018.26.2.151>
- Shen, H. and Hou, C. (2011), “SIFs of CCT plate repaired with single-sided composite patch”, *Fatigue Fract. Eng. M.*, **34**(9), 728-733. <https://doi.org/10.1111/j.1460-2695.2011.01569.x>
- Shen, D.J., Yang, Q., Huang, C.B., Cui, Z.H. and Zhang, J.Y. (2019), “Tests on seismic performance of corroded reinforced concrete shear walls repaired with basalt fiber-reinforced polymers”, *Constr. Build. Mater.*, **209**, 508-521.
<https://doi.org/10.1016/j.conbuildmat.2019.02.109>
- Sih, G.C. (1973), *Handbook of Stress Intensity Factors*, Lehigh University Press, Bethlehem, PA, USA.
- Sun, C.T., Klug, J. and Arendt, C. (1996), “Analysis of cracked aluminum plates repaired with bonded composite patches”, *AIAA J.*, **34**(2), 369-374. <https://doi.org/10.2514/3.13073>
- Wang, H.T. and Wu, G. (2018a), “Bond-slip models for CFRP plates externally bonded to steel substrates”, *Compos. Struct.*, **184**, 1204-1214.
<https://doi.org/10.1016/j.compstruct.2017.10.033>
- Wang, H.T. and Wu, G. (2018b), “Crack propagation prediction of double-edged cracked steel beams strengthened with FRP plates”, *Thin-Wall. Struct.*, **127**, 459-468.
<https://doi.org/10.1016/j.tws.2018.02.018>
- Wang, H.T., Wu, G. and Wu, Z.S. (2014), “Effect of FRP configurations on the fatigue repair effectiveness of cracked steel plates”, *J. Compos. Constr.*, **18**(1), 04013023.
[https://doi.org/10.1061/\(ASCE\)CC.1943-5614.0000422](https://doi.org/10.1061/(ASCE)CC.1943-5614.0000422)
- Wang, H.T., Wu, G. and Jiang, J.B. (2016a), “Fatigue behavior of cracked steel plates strengthened with different CFRP systems and configurations”, *J. Compos. Constr.*, **20**(3), 04015078.
[https://doi.org/10.1061/\(ASCE\)CC.1943-5614.0000647](https://doi.org/10.1061/(ASCE)CC.1943-5614.0000647)
- Wang, H.T., Wu, G., Dai, Y.T. and He, X.Y. (2016b), “Experimental study on bond behavior between CFRP plates and steel substrates using digital image correlation”, *J. Compos. Constr.*, **20**(6), 04016054.
[https://doi.org/10.1061/\(ASCE\)CC.1943-5614.0000701](https://doi.org/10.1061/(ASCE)CC.1943-5614.0000701)
- Wang, H.T. Wu, G. and Pang, Y.Y. (2018), “Theoretical and numerical study on stress intensity factors for FRP-strengthened steel plates with double-edged cracks”, *Sensors*, **18**(7), 2356.
<https://doi.org/10.3390/s18072356>
- Wei, Y., Zhang, X., Wu, G. and Zhou, Y.F. (2018), “Behaviour of concrete confined by both steel spirals and fiber-reinforced polymer under axial load”, *Compos. Struct.*, **192**, 577-591.
<https://doi.org/10.1016/j.compstruct.2018.03.041>
- Wu, G., Wang, H.T., Wu, Z.S., Liu, H.Y. and Ren, Y. (2012), “Experimental study on the fatigue behavior of steel beams strengthened with different fiber-reinforced composite plates”, *J. Compos. Constr.*, **16**(2), 127-137.
[https://doi.org/10.1061/\(ASCE\)CC.1943-5614.0000243](https://doi.org/10.1061/(ASCE)CC.1943-5614.0000243)
- Wu, C., Zhao, X.L. and Al-Mahaidi, R. (2013), “Mode I stress intensity factor of center-cracked tensile steel plates with CFRP reinforcements”, *Int. J. Struct. Stab. Dy.*, **13**(1), 1350005.
<https://doi.org/10.1142/S0219455413500053>
- Ye, H.W., Li, C.J., Pei, S.L., Ummenhofer, T. and Qu, H.B. (2018), “Fatigue performance analysis of damaged steel beams strengthened with prestressed unbonded CFRP plates”, *J. Bridge Eng.*, **23**(7), 04018040.
[https://doi.org/10.1061/\(ASCE\)BE.1943-5592.0001251](https://doi.org/10.1061/(ASCE)BE.1943-5592.0001251)
- Yu, Q.Q., Chen, T., Gu, X.L., Zhao, X.L. and Xiao, Z.G. (2013), “Fatigue behaviour of CFRP strengthened steel plates with different degrees of damage”, *Thin-Wall. Struct.*, **69**, 10-17.
<https://doi.org/10.1016/j.tws.2013.03.012>
- Yu, Q.Q., Zhao, X.L., Chen, T., Gu, X.L. and Xiao, Z.G. (2014a), “Crack propagation prediction of CFRP retrofitted steel plates with different degrees of damage using BEM”, *Thin-Wall. Struct.*, **82**, 145-158. <https://doi.org/10.1016/j.tws.2014.04.006>
- Yu, Q.Q., Zhao, X.L., Xiao, Z.G., Chen, T. and Gu, X.L. (2014b), “Evaluation of stress intensity factor for CFRP bonded steel plates”, *Adv. Struct. Eng.*, **17**(12), 1729-1746.
<https://doi.org/10.1260/1369-4332.17.12.1729>
- Yu, Q.Q. and Wu, Y.F. (2018), “Fatigue retrofitting of cracked steel beams with CFRP laminates”, *Compos. Struct.*, **192**, 232-244. <https://doi.org/10.1016/j.compstruct.2018.02.090>
- Yu, Q.Q., Gu, X.L., Zhao, X.L., Zhang, D.M., Huang, H.W. and Jiang, C. (2019), “Characterization of model uncertainty of adhesively bonded CFRP-to-steel joints”, *Compos. Struct.*, **215**, 150-165. <https://doi.org/10.1016/j.compstruct.2019.02.045>
- Zhang, D., Gu, X.L., Yu, Q.Q., Huang, H.W., Wan, B.L. and Jiang, C. (2018), “Fully probabilistic analysis of FRP-to-concrete bonded joints considering model uncertainty”, *Compos. Struct.*, **185**, 786-806. <https://doi.org/10.1016/j.compstruct.2017.11.058>
- Zheng, Y. (2007), “Experimental and theoretical research on fatigue behavior of steel structures strengthened with CFRP”, Ph.D. Dissertation; Tsinghua University, Beijing, China.

BU